Original article

A strategy for mitigating avian colibacillosis disease using plant growth promoting rhizobacteria and green synthesized zinc oxide nanoparticles

Kainat Masood [a], Humaira Yasmin [a,*], Sidra Batool [a,c], Noshin Ilyas [b], Asia Nosheen [a], Rabia Naz [a], Naeem Khan [d], Muhammad Nadeem Hassan [a], Adil Aldhahrani [e], Fayez Althobaiti [f]

[a] Department of Biosciences, COMSATS University Islamabad (CUI), Islamabad, Pakistan
[b] Department of Botany, PMAS-Arid University Rawalpindi, 46300 Rawalpindi, Pakistan
[c] Research School of Chemistry, Australian National University ACT 2601 Australia
[d] Department of Agronomy, Institute of Food and Agricultural Sciences, University of Florida, Gainesville, FL 32611, USA
[e] Clinical Laboratory Sciences Department, Turabah University College, Taif University, Taif 21995, Saudi Arabia
[f] Department of Biotechnology, College of Science, Taif University, P.O. Box 11099, Taif 21944, Saudi Arabia

ABSTRACT

Avian colibacillosis caused by the zoonotic pathogen *Escherichia coli* is a common bacterial infection that causes major losses in the poultry sector. Extracts of different medicinal plants and antibiotics have been used against poultry bacterial pathogens. However, overuse of antibiotics and extracts against pathogenic strains leads to the proliferation of multi-drug resistant bacteria. Due to their environmentally friendly nature, nanotechnology and beneficial bacterial strains can be used as effective strategies against poultry infections. Green synthesis of zinc oxide nanoparticles (ZnO-NPs) from *Eucalyptus globulus* leaves was carried out in this study. Their characterization was done by UV–vis spectroscopy, X-ray diffraction (XRD), and Fourier transmission infrared spectroscopy (FT-IR) which confirmed their synthesis, structure, and size. *In vitro*, antimicrobial activities of plant leaf extract, ZnO-NPs, and plant growth-promoting rhizobacteria (PGPR) were checked against *E. coli* using well diffusion as well as disc diffusion method. Results proved that the antimicrobial activity of ZnO-NPs and PGPR strains was more enhanced when compared to eucalyptus leaf extract at 36 h. The maximum relative inhibition shown by ZnO-NPs, PGPR strains and eucalyptus leaf extracts was 88%, 67% and 58%, respectively. The effectiveness of ZnO-NPs was also increased with an increase in particle dose and treatment time. The 90 mg/ml of ZnO-NPs was more effective. PGPR strains from all over the tested strains, *Pseudomonas* sp. (HY8N) exhibited a strong antagonism against the *E. coli* strain as compared to other PGPR strains used in this study. However, combined application of PGPR (*Pseudomonas* sp. (HY8N)) and ZnO-NPs augment antagonistic effects and showed maximum 69% antagonism. The study intends to investigate the binding affinity of ZnO-NPs with the suitable receptor of the bacterial pathogen by *in silico* methods. The binding site conformations showed that the ligand ZnO binds with conserved binding site of penicillin-binding protein 6 (PBP 6) receptor. According to the interactions, ZnO-NPs form the same interaction pattern with respect to other reported ligands, hence it can play a significant role in the inhibition of PBP 6. This research also found that combining ZnO-NPs with *Pseudomonas* sp. (HY8N) was a novel and effective technique for treating pathogenic bacteria, including multidrug-resistant bacteria.

© 2021 The Authors. Published by Elsevier B.V. on behalf of King Saud University. This is an open access article under the CC BY-NC-ND license (http://creativecommons.org/licenses/by-nc-nd/4.0/).

1. Introduction

Microbes are involved in many acute and chronic diseases in both poultry and humans (Heredia and García, 2018). The most common infectious disease of poultry is avian Colibacillosis, which is caused *by E. coli* (*Escherichia coli)* and is linked to significant economic losses in the poultry industry (Xing et al., 2020). The Avian *Colibacillosis* was found widely prevalent in all age groups of chickens (9.52 to 35.73%) with an especially high prevalence rate in adult birds (36.73%) While *E. coli* is a natural part of the chicken's

Production and hosting by Elsevier

intestinal micro flora, pathogenic *E. coli* strains colonizing the respiratory tract cause morbidity and mortality in poultry (Coura et al., 2017). It also cause damage to the reproductive tract of chicken and adversely affect chicken fertility (Coura et al., 2017). Several essential oils of medicinal plants and antibiotics have demonstrated antimicrobial activity to treat diseases (Habibi et al., 2018; Millezi et al., 2019). However, several problems are related to these strategies like the sensitivity of essential oils to oxygen, moisture, light, and temperature and antibiotics-related drug resistance in pathogens. These characteristics could diminish their antimicrobial activity (Chouhan et al., 2017). Antibiotic use is common, which creates a vital pressure that contributes to antimicrobial resistance in *Colibacillosis* (Afshin Zakeri, 2012). Antimicrobial-resistant *E. coli* strains may be spread to humans through the food chain or through direct contact with infected birds, posing significant health risks (Ibrahim et al., 2019). One of the effective ways to control bacterial pathogens is metal oxide nanoparticles (NPs) (Jamil et al., 2016).

NPs are small molecules that are 1–100 nm, used in health, food, chemical, cosmetic industries, and agriculture (Farhangi-Abriz and Torabian, 2018). NPs having antioxidant and antimicrobial contents are considered as a new shift of antimicrobial therapeutic agents for the preservation of food and killing pathogenic microorganisms (Dadi et al., 2019). NPs act as a promising solution for resistance to antimicrobial agents (Sánchez-López et al., 2020). Since NPs have coordinated contact with the bacterial cell wall without having to reach the cell, they may be less susceptible to fostering bacterial resistance than antibiotics. (Wang et al., 2017). Like antibiotics, metal oxides act against microorganisms through different mechanisms such as membrane breakdown, damage of cellular components (protein, DNA, and electron transport chain), and generation of reactive oxygen species (ROS) (Sánchez-López et al., 2020). NPs consisting of (Fe_3O_4, TiO_2, CeO, CuO, and ZnO) metal oxide has strong antibacterial efficiency (Dadi et al., 2019; Jin and Jin, 2021). Most researchers concentrate on the green synthesis of metal oxide NPs. Biological synthesis of NPs by using the plant is a fast and low-cost option and is safe for human use (Elumalai et al., 2015; Yang et al., 2017).

Different plant extracts have been used to make ZnO-NPs (Elumalai et al., 2015; Sánchez-López et al., 2020; Singh et al., 2018). The antibacterial activities of ZnO-NPs are known against gram-negative and gram-positive. (Dadi et al., 2019; Sánchez-López et al., 2020), (Salgado et al., 2019) have reported the green synthesis of metal oxide NPs from the eucalyptus plant. The chemicals present in eucalyptus leaf extract have been described to cause diminishment of metal ions to NPs and, eventually wipe out the use of noxious chemicals, high pressure, temperature, energy, and maintenance of microbial growth cultures (Salgado et al., 2019).

ZnO-NPs have a strong binding affinity with proteins, hydrogen, and metal receptors. Computational analysis or *In silico* approach is used to understand the mechanism of NPs for their cytotoxicity/antimicrobial activity against microbes on the molecular level. Penicillin-binding proteins are primarily responsible for the synthesis and remodelling of the bacterial cell wall among bacterial targets (PBPs) (Macheboeuf et al., 2006), (Sauvage et al., 2008). These targets serve as primary targets of the β-lactam antibiotics and have been the focus of intense mechanistic, structural, and medicinal chemistry research. There are two primary DD-carboxypeptidases in Escherichia coli, PBP5 and PBP6 (Ghosh et al., 2008), which together account for 85% of the copy numbers of all PBPs (Tamura et al., 1976). Unlike PBP5, few studies have been conducted on PBP6, and the biological functions of these DD-carboxypeptidases are unknown (Spratt and Strominger, 1976). So, for this study the 3D structure of PBP6 has been taken as a receptor.

PGPR living in association with plant roots have been reported to display antagonism against soil-borne phytopathogens by producing several substances (Beneduzi et al., 2012). These biocontrol agents produce lytic enzymes (glucanase, pectinase, chitinase, amylase etc.), siderophores, and antibiotics to impede the growth of harmful agents (Yasmin et al., 2020). Antagonistic activities of ZnO-NPs prepared from different plant extracts have been reported. However, information is scanty about the efficacy of ZnO-NPs prepared from eucalyptus and PGPR to antagonize *E. coli* strain causing Colibacillosis in poultry. The main objectives of the present study were the green synthesis and characterization of NPs from eucalyptus and their minimum inhibitory dose to induce toxicity against *E. coli*. Moreover, the antagonistic activity of plant growth-promoting bacteria against *E. coli* was observed. An *in-silico* approach was used to find the predictive model for virtual screening of how NPs use to control *Colibacillosis* to forecast how a ligand (ZnO-NPs) interacts with the receptor (Penicillin binding protein) of *E. coli*.

2. Materials and methods

2.1. Accession of cultures

Stock culture of *E. coli* ST131-H22 was obtained from Poultry Graduate Research Institute Rawalpindi. Five strains of PGPR (*Pseudomonas* sp. (HY8N), *Bacillus pumilus* (HYJW), *Bacillus cereus* (HY9K), *Pseudomonas* sp. (HY13KI), and *Pseudomonas* sp. (HY13KR), were accessed from Applied Microbiology and Biotechnology Lab, COMSATS University, Islamabad. The accession number of all the bacterial strains used in this study are displayed in table 1. These bacterial cultures were revived on LB agar plates for further use.

2.2. Antibacterial activity assay

2.2.1. Preparation of the cell-free bacterial suspension

The method described by (Yasmin et al., 2017b) was followed to prepare cell-free bacterial suspensions. All the PGPR strains and test organisms (*E. coli*) were inoculated in LB broth and placed in a shaking incubator to reach their log phase at 37 °C. After enough growth for each strain, cells were separated from the media after centrifugation at 9000 rpm for 10 min. The supernatant was discarded, and the pellet was suspended in sterilized distilled water for further use in well diffusion and disc diffusion methods.

2.2.2. Well diffusion assay

The antagonistic potential of PGPR was determined using the well diffusion assay. The cell-free bacterial suspension of pathogenic strain (10^7 CFU/ml) was evenly spread as a lawn on sterilized agar plates with an autoclaved cotton bud. The wells of 6 mm diameter were punched with a sterilized cork borer. Then, 100 μl of inoculum containing 10^6 CFU/ml of each five different PGPR strains (*Pseudomonas* sp. (HY8N), *Bacillus pumilus* (HYJW), *Bacillus cereus* (HY9K), *Pseudomonas* sp. (HY13KI), and *Pseudomonas* sp. (HY13KR) was added in the wells. The plates were then incubated at 32 °C for 3–4 days. After incubation, the diameters of the inhibi-

Table 1
List of bacterial strains with their accession numbers used in this study.

Strains	Accession numbers	References
Bacillus pumilus HYJW	KT 003271.1	Yasmin et al., 2017a
Pseudomonas sp. HY8N	KF307196	Yasmin et al., 2017a
Bacillus cereus HY9K	DQ289055	Yasmin et al., 2017a
Pseudomonas sp. 13KI	KJ191560	Yasmin et al., 2017a
Pseudomonas sp. HY13KR	KF307201	Yasmin et al., 2017a
Escherichia coli	PRJNA407956	Not published

tion zones of *E. coli* formed around the wells were recorded. Three replicates were carried out for each bacterial strain. LB agar plates with inoculation of *E. coli* pathogenic strain and standard antibiotic discs of tetracycline and gentamicin were used as the positive controls.

2.2.3. Disc diffusion assay

In the disc diffusion method discs of autoclaved filter paper saturated with different bacterial suspensions were placed on a lawn of pathogenic bacteria on an agar medium (as described in the previous section). The plates were then incubated in the incubator for 2–3 days at 30 °C. The zone of inhibitions formed around the discs due to antagonistic activity of PGPR strains was measured. LB agar plates with inoculation of *E. coli* pathogenic strain and standard antibiotic discs of tetracycline and gentamycin were used as the positive controls.

2.2.4. Calculation of relative inhibition percentage

The following formula was used to measure the relative percentage inhibition of cell-free bacterial culture for the positive regulation.

$$Relative\ percentage\ inhibition\ =\ 100 \times (Z - Y)\tilde{A} \cdot (X - Y)$$

where, X = total area of inhibition of the tested strain, Y = total area of inhibition of the inoculated LB broth, Z = total area of inhibition of the standard drug.

2.3. Preparation of leaf extract

Aqueous leaves extracts of eucalyptu**s** were prepared by collecting fresh leaves of eucalyptu**s** from the Mianwali district. The leaves were thoroughly washed under running water with distilled water to remove dirt and impurities and allowed to completely dry in a shadow place for 25 to 30 days. After drying the samples were ground into fine powder in the kitchen blender. For the preparation of aqueous leaf extract, 10 g of dry leaf powder was added to 100 ml of distilled water. The mixture was then put on a hot plate at 60 °C for 30 min while being constantly stirred. The aqueous mixture was filtered using Whatman filter paper after cooling to room temperature and the extract was kept at 4 °C.

2.4. Antimicrobial assay of plant extracts

An antimicrobial assay of extracts of eucalyptus leaves was performed by the well diffusion method. The lawn of the test organism (*E. coli*) and wells on culture plates was prepared as described above. Then, plant extracts of 5 mM, 10 mM, 15 mM, and 20 mM, concentration were added into 6 mm wells and allowed to diffuse for 30 min at room temperature. After incubation for 12–36 h at 37 °C, a clear zone of inhibition around the wells exhibiting the antimicrobial activity of extracts against the tested organism was recorded.

2.5. Synthesis of ZnO-NPs

The method of Elumalai *et al.* (Elumalai et al., 2015) was used for the green synthesis of ZnO-NPs from leaf extracts of eucalyptus. On a magnetic stirrer, the 30 ml of crude plant extract was heated at 60 °C. When the temperature of the extract rose to 60 °C, 3 mg of zinc nitrate hexahydrate (Zn (NO$_3$)$_2$·6H$_2$O) was added and kept for 1 h till the formation of white precipitates. This mixture was then left for 24 h till a smooth paste developed in a hot air oven at 60 °C. This paste was rinsed multiple times with a distilled water: ethanol (3:1) solution. The paste was then moved to a ceramic crucible

cup and heated in the oven at 400 °C for 2 h. In an airtight bag, the resulting white powder was treated for characterization.

2.6. Characterization of ZnO-NPs

The reduction of Zn$^+$ ions was tracked after diluting a small sample into distilled water by measuring the UV–vis spectrum at a wavelength of 200–800 nm using the UV– vis spectrophotometer UV-1800. Fourier transforms infrared (FTIR) spectral measurements were used to identify the potential biomolecules in eucalyptus leaf extract which is responsible for reducing and capping the bio-reduced ZnO-NPs. The ZnO-NPs were analyzed for size and crystalline structure by using X-ray diffraction (XRD). XRD provides information about the crystalline structure, nature of the phase, lattice parameters, and crystalline grain size.

2.7. Antibacterial assay

The antibacterial effects of ZnO-NPs were studied by well as well as disc diffusion assay. Different concentrations of ZnO-NPs (10 mg/ml, 30 mg/ml, 60 mg/ml, and 90 mg/ml) were formed by dissolving them in autoclaved distilled water by ultra-sonication in a sonicator for 10 min and at 40HZ. The lawn of test strain (*E. coli*) was prepared by the same methods for filter disc and well diffusion assay was the same as described in the previous section.

In each plate, sterile paper discs of 6 mm diameter (dipped in 25 mg/ml ZnO-NPs) were mounted alongside two control antibiotic-containing discs for the disc diffusion antagonistic assay. Overnight at 32 °C, the cultured agar plates were incubated. In a well diffusion assay, all concentrations of ZnO-NPs (100 μl) were added into each well (6 mm) on the lawn of the tested strain and incubated at 37 °C for 24 h. The inhibition zones around the well were recorded**.**

2.8. Co-application of PGPR and ZnO-NPs

For co-assay sterile paper discs made of Whatman filter paper (6 mm diameter) were soaked in 5 ml of PGPR (10^6 cfu/ml) and ZnO-NPs (25 mg/ml). After that, these discs were dried and placed in the lawn of tested pathogenic strain. After overnight incubation at 32 °C the inhibition zones around the discs were recorded after 12 h, 24 h and 36 h.

2.9. Molecular docking

After the characterization of ZnO-NPs, the study intends to investigate the binding affinity of this ligand with any suitable bacterial receptor by *in silico* methods. The interactions between ZnO-NPs as ligand and PBP6 protein as receptor were simulated using molecular docking. The related protein data bank is taken from the RCSB protein data bank (PDB) (Berman et al., 2000) entry was searched for PBP6. For molecular docking, the crystal structure of penicillin-binding protein 6 (PBP6) from E. coli (PDB ID: 3ITA) was chosen. After receptor selection, the successful identification of binding pocket residues is important to find out the interactions between ligand and receptor. This step is very crucial in computational methods and used for target drug designing. The detailed binding pocket analysis has been reported for PBP6 (Chen et al., 2009) and given in Table 2.

The binding site residues are mostly present in the C-terminal domain of penicillin-binding protein 6. This domain's active site configuration and topography are similar to those of class A-lactamases. (Nukaga et al., 2008). Graphically the position of different active sites in the 3D structure of penicillin-binding protein 6 is shown in Fig. 1. The residues of each binding pocket are focused and represented in Fig. 2.

Table 2
Comparison of the zone of inhibition produced by PGPRs strains against *E. coli* in well diffusion and disk diffusion method. All such means which share a common English letter are similar, otherwise, they differ significantly p ≤ 0.05.

Treatments	Well diffusion method			Disk diffusion method		
	Zone of inhibition (mm)			Zone of inhibition (mm)		
	12 h	24 h	36 h	12 h	24 h	36 h
Bacillus pumilus (HYJW)	4.5 ± 0.01f	5 ± 0.02e	6.5 ± 0.02c	5 ± 0.02de	5.5 ± 0.01d	7 ± 0.01c
Bacillus cereus (HY9K)	3 ± 0.01 g	3.5 ± 0.01 g	4.5 ± 0.01f	3.5 ± 0.01 g	4 ± 0.01ef	5 ± 0.01
Pseudomonas sp. (HY8N)	6 ± 0.02 cd	7 ± 0.02b	8 ± 0.03a	7 ± 0.01c	8 ± 0.02b	8.5 ± 0.02a
Pseudomonas sp. (HY13KI)	3.5 ± 0.014 g	4 ± 0.01f	4.5 ± 0.02f	3.5 ± 0.01 g	4 ± 0.01ef	4.5 ± 0.01e
Pseudomonas sp. (HY13KR)	2 ± 0.01 h	2.5 ± 0.01 h	3 ± 0.01 g	3 ± 0.01 h	3.5 ± 0.01	4 ± 0.01e

Different letters signifies significant variations at LSD (P = 0.05), n = 3 and ± indicates standard error between three replicates
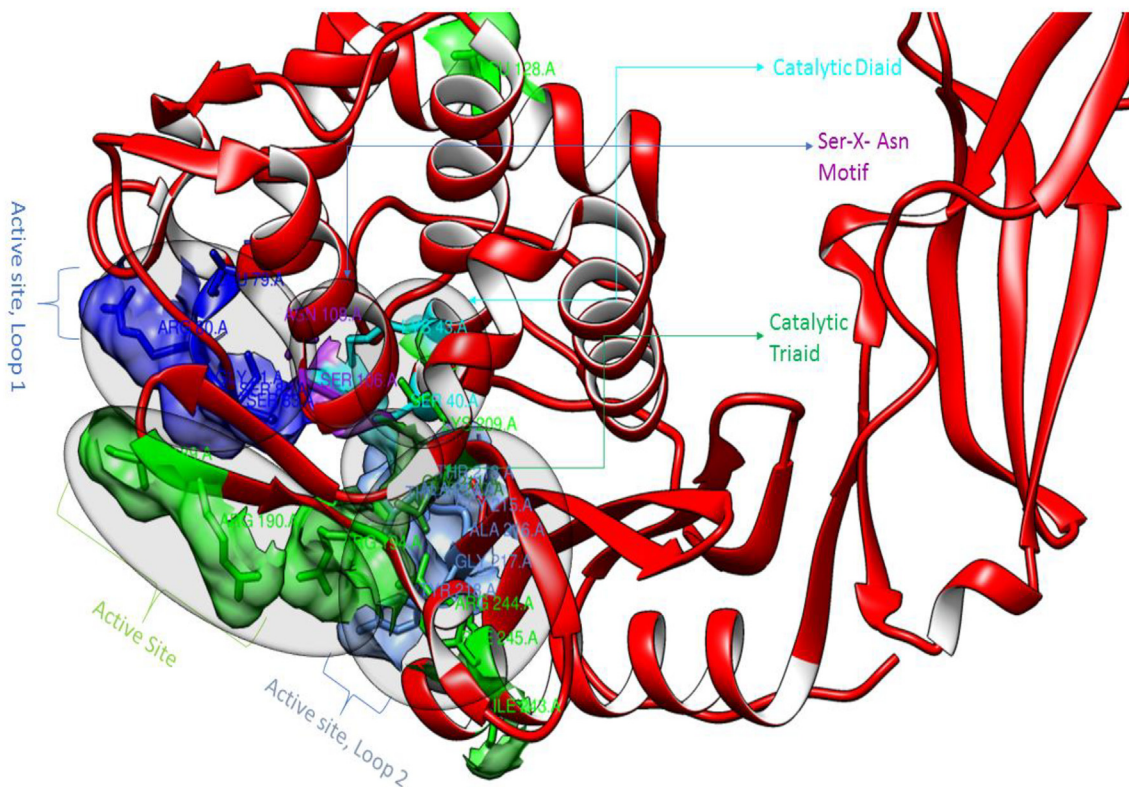
Fig. 1. Detailed overview of binding site residue positions in the 3D structure of 3ITA.

3D structures of ligand ZnO-NPs were obtained from PubChem (Kim et al., 2019). The molecular docking study was performed between ligand and receptor by using PyRx Autodock vina version 0.8. window available (http://pyrx.sourceforge.net) . All parameters for the vina grid and spacing are given in Table 3. The number of total 9 runs was set to visualize all the possible confirmations. The grid size was established to cover the entire receptor to find the possible conformations. Furthermore, the docking result was seen by analyzing binding energies and binding interactions between ligand and receptor (Furqan et al., 2020). For post docking, molecular docking analysis Chimera and Ligplot + have been used

2.10. Statistical analyses

The software Statistix version 8.1 was used to analyze data statistically by using the analysis of variance (ANOVA) technique Least Significant Difference (LSD) was used to compare the mean values of the treatments to see if there were any significant differences at P = 0.05 [30].

3. Results

3.1. Antimicrobial assay for PGPR

3.1.1. Well diffusion method

The results of antimicrobial activity revealed that all PGPR strains showed significant antagonistic activity against poultry bacterial pathogen *E. coli*. All five strains of PGPR *Pseudomonas* sp. (HY8N), *Bacillus pumilus* (HYJW), *Bacillus cereus* (HY9K), *Pseudomonas* sp. (HY13KI), and *Pseudomonas* sp. (HY13KR) showed pronounced antagonism against pathogenic strains of *E. coli* in well diffusion methods (Fig. 3). The diameter of the inhibitory zone around the tested strains was increased with an increase in incubation time. The maximum zone of inhibition i.e. 8 mm was exhibited by *Pseudomonas* sp. (HY8N), at 36 h. The pattern of antagonistic activities of different PGPR was *Pseudomonas* sp. (HY8N) < *Bacillus pumilus* (HYJW) < *Bacillus cereus* (HY9K) ≤ *Pseudomonas* sp. (HY13KI) < *Pseudomonas* sp. (HY13KR) with inhibitory zones of 8 mm, 6.5 mm, 4.5 mm, 4.5 mm, 3 mm respectively after 36 h. (Table 4).
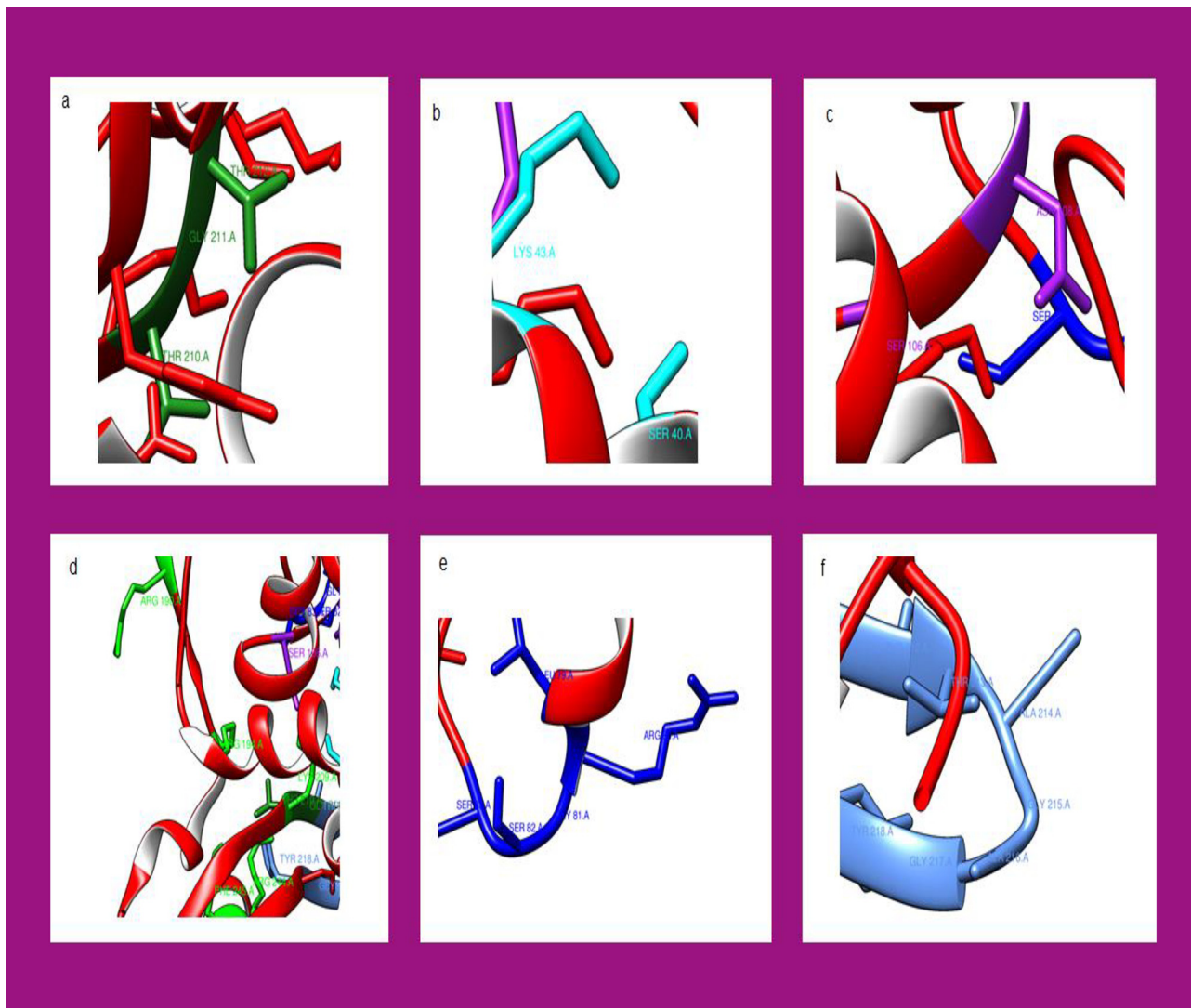
Fig. 2. a) Catalytic Triad, b) Nucleophilic Active site Catalytic Diad, c) (Ser-X-Asn) Motif, d) Active site, e) Active site: Loop 1, f) Active site: Loop 2.

Table 3
Zone of inhibitions of plant extract by well diffusion assay.

Treatments	Well diffusion method		
	Zone of inhibition (mm)		
	12 h	24 h	36 h
T1 (5 mM)	2 ± 0.01 h	4 ± 0.01e	4.5 ± 0.01d
T2 (10 mM)	2.5 ± 0.01 g	4.75 ± 0.01 cd	5 ± 0.01c
T3 (15 mM)	3 ± 0.01f	5 ± 0.01c	5.5 ± 0.01b
T4 (20 mM)	3.5 ± 0.01f	5.5 ± 0.01b	6 ± 0.01a

Different letters signify significant variations at LSD (P = 0.05), n = 3 and ± indicates standard error between three replicates**.**

3.1.2. Disc diffusion method

The disc diffusion assay's findings exhibited significant antimicrobial potentials of all tested PGPR strains against pathogen strain of *E. coli*. The maximum zone of inhibition i.e. 8 mm was exhibited by *Pseudomonas* sp. (HY8N), at 36 h. The pattern of antagonistic activities of different PGPR was *Pseudomonas* sp. (HY8N) < *Bacillus pumilus* (HYJW) < *Bacillus cereus* (HY9K) ≤ *Pseudomonas* sp. (HY13KI) < *Pseudomonas* sp. (HY13KR) with inhibitory zones of 8.5 mm, 7 mm, 5 mm, 4.5 mm, 4 mm respectively, at 36 h (Table 4).

3.1.3. Comparison of relative percentage inhibition of well diffusion and disc diffusion methods

Fig. 4 represents the relative percentage inhibition of all tested PGPR strains against the pathogenic strain of *E. coli* causing avian colibacillosis disease at 12 h, 24 h, and 36 h. All strains showed higher relative inhibition (%) after 36 h of incubation as compared to 12 h and 24 h in both well diffusion and disc diffusion assays. Overall, the results of the disc diffusion method manifest higher % inhibition of all PGPR strains than the well diffusion. Results exhibited that *Pseudomonas* sp. (HY8N) showed maximum relative percentage inhibition of 55% in well diffusion and 65% in disc diffusion assay at 36 h of incubation as compared to the non-treated control.

3.2. Characterization of NPs

3.2.1. UV–Vis spectral analysis

The UV–Vis spectrum of ZnO-NPs shown in Fig. 3 initially confirmed the synthesis of NPs from eucalyptus leaf extracts. The spectra for ZnO-NPs were observed between 200 and 800 nm range. At 360 nm, the absorption peak of ZnO-NPs was observed. It was observed that the peak was shifted from 300 to 460 nm that indicated that the particles are polydisperse (Fig. 6).
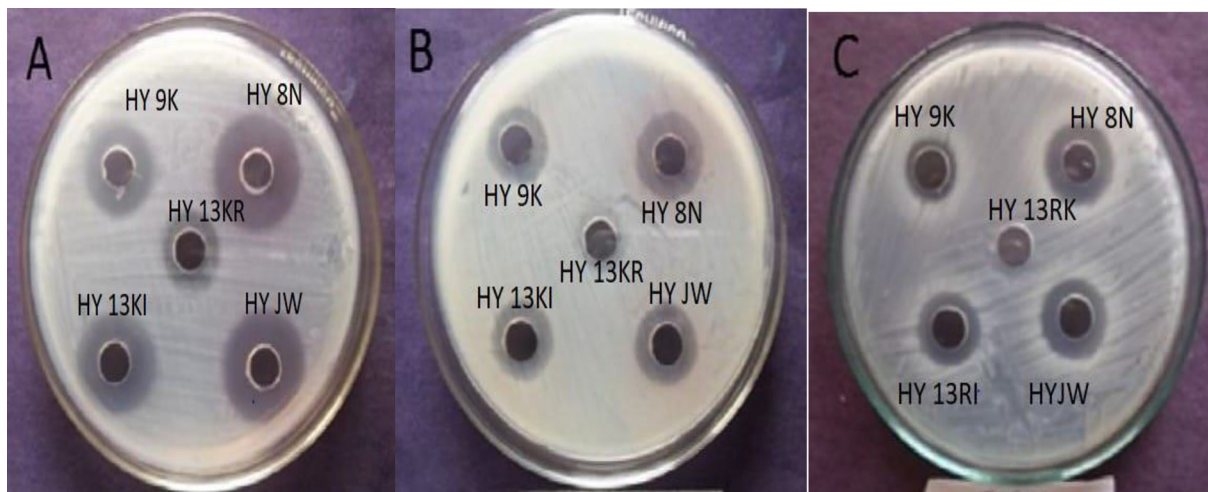
Fig. 3. Antagonistic activities of different strains of PGPRs against a pathogenic strain of *E. coli* of Colibacillosis disease by disk diffusion assays A) 36 h B) = 24 h, C) = 12 h.

Table 4
Comparison of the zone of inhibition produced by different concentrations of ZnO-NPs synthesized from eucalyptus leaf extract against *E. coli* in well diffusion and disc diffusion method.

Treatments	Well diffusion method			Disc diffusion method		
	Zone of inhibition (mm)			Zone of inhibition (mm)		
	12 h	24 h	36 h	12 h	24 h	36 h
T1	3 ± 0.01j	4.5 ± 0.01i	5 ± 0.01 h	3 ± 0.01 g	4 ± 0.01e	4.5 ± 0.01d
T2	5 ± 0.01 h	5.5 ± 0.01 g	6 ± 0.02f	3.5 ± 0.01f	4.5 ± 0.012d	5.5 ± 0.02c
T3	6 ± 0.01f	7 ± 0.02e	8 ± 0.01c	4 ± 0.01e	5.5 ± 0.02c	6.5 ± 0.02b
T4	7.5 ± 0.02d	8.5 ± 0.01b	9 ± 0.02a	5 ± 0.02c	6.5 ± 0.021b	7 ± 0.025a

Whereas, T1= (10 mg/ml), T2= (30 mg/ml), T3= (60 mg/ml), T4= (90 mg/ml) concentrations of ZnO-NPs. Different letters signifies significant variations at LSD (P = 0.05), n = 3 and ± indicates standard error between three replicates.

3.2.2. FT-IR analysis

The FTIR analysis of ZnO-NPs was done to identify different bio-molecules responsible for reduction and stabilization of ZnO-NPs. FTIR spectra of ZnO-NPs synthesized from eucalyptus plant extract by green method displayed in Fig. 4 showed that the leaves extract of eucalyptus had stabilizing agents. The spectra for FT-IR analysis were recorded in the 4000–500 cm^{-1} range. In FT-IR spectra the bands were observed at 1646 and 1548 cm^{-1} indicated stretching and bending vibration of bonds. The band formed at 443 cm^{-1} shows the presence of C = C-C and carbon –carbon double bond aromatic groups. The strong bands at 1548 and 1384 cm^{-1} showed the presence of glycosidic linkage of C-O-C alcoholic groups in ZnO-NPs (Fig. 6).

3.2.3. X-ray diffraction (XRD) chromatography

The XRD spectra of ZnO-NPs synthesized from eucalyptus leaf extract were shown in Fig. 5. All the peaks were hexagonal. Also, ZnO-NPs have a stable crystallographic stage. The sharp diffraction peaks were observed at 2θ values 32.63, 33.36, 37.07, 47.46, 62.84, 68.11°. High width of peaks was observed due to the increase in quantum number confirmed using JCPDS card number 36–1450. The average particle size of ZnO was 36 mm calculated using the Scherer equation (Fig. 6).

3.3. Antimicrobial activity by crude leaf extract of eucalyptus

The plant extract of eucalyptus showed significant antimicro-bial activity against poultry bacterial pathogen *E. coli*. All the con-centrations (5 mM, 10 mM, 15 mM, and 20 mM) of eucalyptus leaf extract showed inhibitory zones against pathogenic strains of *E. coli*. As the concentration of extract was increased, the diameter of the inhibitory zones grew. The maximum zone of inhibition i.e. 8 mm was exhibited by 20 mM concentration of leaf extract at 36 h. The pattern of antimicrobial activities of different concentra-tions of crude leaf extract was 5 mM < 10 mM < 15 mM < 20 mM with inhibitory zones of 6 mm, 6.5 mm, 7 mm, and 8 mm, respec-tively at 36 h (Table 5).

3.4. Evaluation of the bioactivity of ZnO-NPs against pathogenic strains of E. Coli

3.4.1. Well diffusion method

The findings revealed that the ZnO-NPs showed significant antimicrobial activity against poultry bacterial pathogen *E. coli*. All the concentrations (10 mg/ml, 30 mg/ml, 60 mg/ml and 90 mg/ml) of ZnO-NPs produced prominent inhibitory zones against pathogenic strains of *E. coli*) (Fig. 7). However, as the con-centration of NPs increased, the diameter of the inhibitory zones grew. The maximum zone of inhibition i.e. 7 mm was exhibited by 90 mg/ml concentration of ZnO-NPs at 36 h. The pattern of antimicrobial activities of different concentrations was 10 mg/ml < 30 mg/ml < 60 mg/ml < 90 mg/ml with inhibitory zones of 5 mm, 6 mm, 8 mm, and 9 mm, respectively at 36 h (Table 6).

3.4.2. Disc diffusion assay

The results of the antibacterial activity revealed that the ZnO-NPs showed significant antimicrobial activity against poultry bac-terial pathogen *E. coli*. All the concentrations (10 mg/ml, 30 mg/ml, 60 mg/ml and 90 mg/ml) of ZnO-NPs showed an inhibitory zone against pathogenic strains of *E. coli* (Fig. 8). However, the diameter
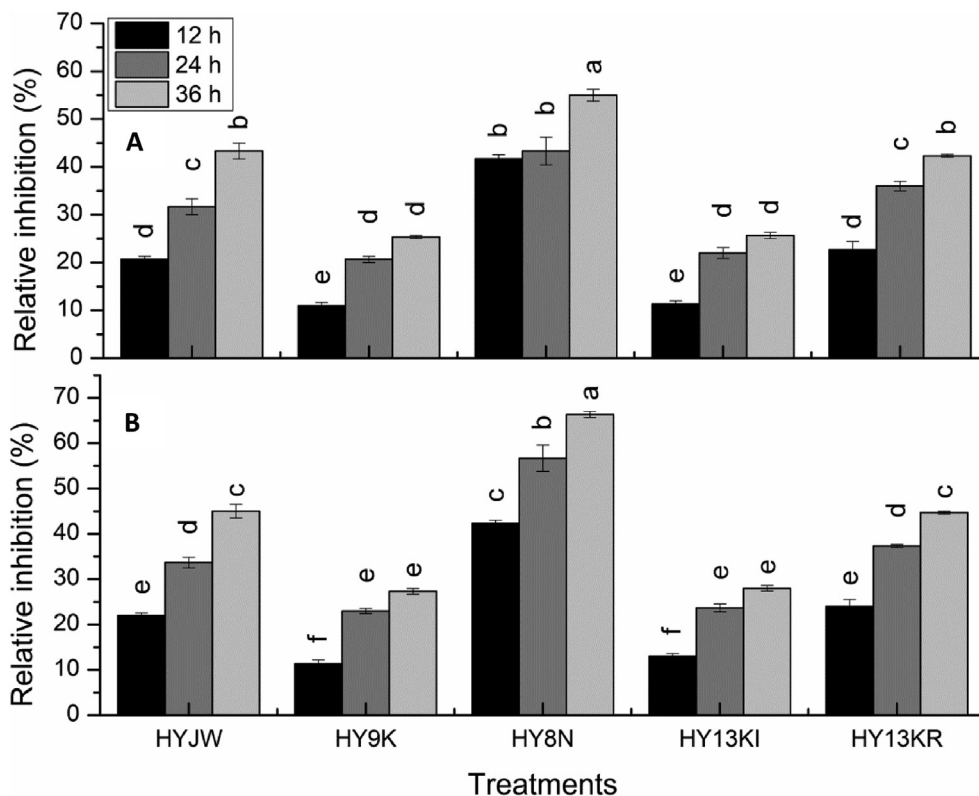
Fig. 4. Relative percentage inhibition of PGPR strains against pathogenic strain of *E. coli* causing avian colibacillosis disease at 12 h, 24 h and 36 h of incubation A) Well diffusion assay B) Disc diffusion assay. Different letters signifies significant variations at LSD (P = 0.05), n = 3 and ± indicates standard error between three replicates. Whereas, HYJW = *Bacillus pumilus*, HY9K = *Bacillus cereus*, HY8N, HY13KI and HY13KR = *Pseudomonas* sp.
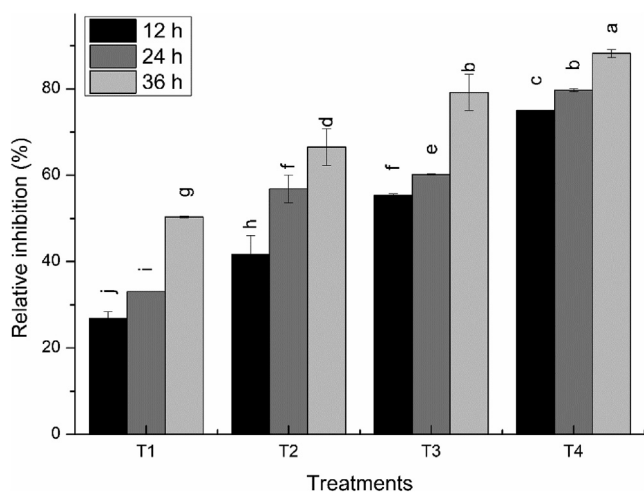
Fig. 5. Relative percentage inhibition of different concentrations of plant extract against the pathogenic strain of *E. coli*. A) Well diffusion method B) Disc diffusion method, Whereas, T1 = 5 mM, T2 = 10 mM, T3 = 15 mM, T4 = 20 mM concentrations of ZnO-NPs. Different letters signify significant variations at LSD (P = 0.05), n = 3 and ± indicates standard error between three replicates.

3.4.3. Comparison of relative percentage inhibition of well diffusion and disc diffusion methods

The relative percentage inhibition of all tested concentrations (10 mg/ml, 30 mg/ml, 60 mg/ml, and 90 mg/ml) of ZnO-NPs against the pathogenic strain of *E. coli* at 12 h, 24 h, and 36 h are shown in Fig. 8. After 36 h of incubation, all concentrations exhibited higher relative inhibition (%) than 12 h and 24 h, in both well diffusion and disc diffusion methods. Overall, the results of the well diffusion method evidenced more % inhibition of all tested concentrations than the disc diffusion. Results exhibited that 90 mg/ml of ZnO-NPs showed maximum relative percentage inhibition of 82% in well diffusion and 76% in disc diffusion assay after 36 h of incubation as compared to the non-treated control.

3.4.4. Co application of PGPR and ZnO-NPs as antagonist

The results of antimicrobial activity revealed that the combined application of PGPRs and ZnO-NPs showed significant antibacterial activity against poultry bacterial pathogen *E. coli*. All five strains of PGPRS *Pseudomonas* sp. (HY8N), *Bacillus pumilus* (HYJW), *Bacillus cereus* (HY9K), *Pseudomonas* sp. (HY13KI), and *Pseudomonas* sp. (HY13KR) showed marked antagonism with best dose 90 mg/ml of ZnO-NPs (Fig. 9). However, the diameter of the inhibitory zone was increased with an increase in incubation time. The maximum zone of inhibition i.e. 67 mm was exhibited by *Pseudomonas* sp. (HY8N) with 90 mg/ml concentration of ZnO-NPs, at 36 h. The pattern of antagonistic activities of different PGPRs with 90 mg/ml concentration of ZnO-NPs was *Pseudomonas* sp. (HY8N) < *Bacillus pumilus* (HYJW) < *Bacillus cereus* (HY9K) ≤ *Pseudomonas* sp. (HY13KI) < *Pseudomonas* sp. (HY13KR) with inhibitory zones of 67 mm, mm, 47 mm, 45 mm, 29 mm and 28 mm respectively at 36 h (Fig. 9).

of the inhibitory zones was increased with an increase in the concentration of NPs and incubation time. The maximum zone of inhibition i.e. 9 mm was exhibited by 90 mg/ml concentration of ZnO-NPs at 36 h. The pattern of antimicrobial activities of different concentrations was 10 mg/ml < 30 mg/ml < 60 mg/ml < 90 mg/ml with inhibitory zones of 4.75 mm, 5.5 mm, 6.5 mm, and 7 mm, respectively at 36 h (Table 6).

Fig. 6. Characterization of ZnO-NPs synthesized from Eucalyptus leaf extract A) UV–vis analysis B) FT-IR analysis of ZnO-NPs prepared from Eucalyptus leaf extract C) XRD analysis.

3.5. Post docking analysis

Molecular dockings were performed between PBP6 receptor and ZnO-NPs using Autovina Pyrx plugin. The energy values were used to operate the docking conformations; thus, the first structure corresponds to the lowest energy conformation. The free energy of a complex has a direct relationship with its overall stability. Lower energy values indicate that the ligand and receptor have a high binding affinity. In order to determine the effective complex cre-

ation, it is critical to emphasise each complex's free energy. Each complex was then analyzed on Ligplot to identify the binding residues of the receptor.

The ligand ZnO binds to the conserved binding site of the penicillin binding Protein 6 receptor, according to a detailed study of the binding site conformations. The overall binding pattern of each conformation for ZnO is described in Table 7. Graphically the interactions can be represented in Fig. 10. It is reported in the literature that the substrate NAM-(L-Ala-D-isoGlu-L-Lys-D-Ala-D-Ala) binds

Table 5
Binding pockets of selected PBP6 having a PDB id: 3ITA.

Active site classification	Binding Residues
Catalytic Triad	Thr210, Gly211, Thr212,
Active Site	Leu128, Ile189, Arg190, Arg194, Lys209, Ile243, Arg244, Phe245
Active site Loop 1	Active site loops: Loop1: Leu79, Arg80, Gly81, Ser82, Ser83
Active site Loop2	Thr212, Thr213, Ala214, Gly215, Ala216, Gly217, Tyr218
(Ser-X-Asn) Motif	Ser106, Asn108,
Nucleophilic Active site Catalytic Diad (Ser-X-X-Lys)	Ser40, Lys43

with key catalytic dyad residues, such as Ser40 and Lys43 of PBP6. Also, it exhibits interactions with Ser106, Thr210, Arg244, Thr212, and active site loop 1 residue 81–83. The ligand ampicillin also shows interactions with catalytic diad Ser40, Lys43, and (Ser-X-Asn) Motif residues Ser106, Asn108, active site residue Arg244, Thr212 of the catalytic triad and active site loop 2 residues. Another group of substrates called carboxypeptidases exhibits interaction with catalytic dyad Ser40, Lys43, (Ser-X-Asn) Motif residue Ser106, catalytic triad residues Thr210, Thr212, active site residues Arg194 and Arg244, active site loop 1 residue 79–83 and active site loop 2 residues ranged from 212 to 218.

4. Discussion

Colibacillosis, caused by the gram-negative bacteria *E. coli*, is the leading cause of chicken mortality worldwide. ts association with various disease conditions, either as a primary pathogen or as a secondary pathogen, has been linked to significant economic losses in the poultry industry (Afshin Zakeri, 2012). Several essential oils of medicinal plants and antibiotics have demonstrated antimicrobial activity to treat bacterial diseases, disease blockage (Habibi et al., 2018). The nonselective use of antibiotics against poultry pathogens and oversensitivity of plant extracts causes the development of antimicrobial resistance in *E. coli* that result from failures in the treatment of disease (Habibi et al., 2018). Therefore, in this research, we showed that the utilization of PGPR strains and ZnO-NPs from eucalyptus leaves revealed strong antimicrobial activity against pathogenic strains of *E. coli*. These methods can be used to achieve a cost-effective and eco-friendly alternative to conventional methods.

Eucalyptus has been used for medicine, ornament purposes, cosmetics, food, and the pulp industry since ancient times. Some constituents extracted from eucalyptus leaf illustrated antimicro-

bial and anti-inflammatory activities including (1, 8-cineole eucalyptol) (Vecchio et al., 2016), a-Pinene, 8-Pinene, Sabinene (Dellacassa et al., 1990), ZnO (Ahmad et al., 2020), FeO₂, and Ag (Salgado et al., 2019). This study revealed that eucalyptus leaf extract showed antimicrobial activity against *E. coli* causing colibacillosis disease in poultry. We found some limitations in using eucalyptus leaf extract, such as low water solubility or need high temperature for solubilization and low stability, and in-store extract spoilage occurs within a week. Our results are in accordance with the findings of Sánchez-López (Sánchez-López et al., 2020) who mentioned that plant extract has a wide range of antimicrobial potential, but that it has some disadvantages, such as a strong organoleptic taste, low water solubility, and low temperature stability. Zinc oxide (ZnO) is a well-engineered compound that has great interest worldwide due to its distinguishing properties and usages in various fields, such as pharmaceuticals, the make-up industry, and photocatalysis (Sánchez-López et al., 2020; Singh et al., 2018). Nanotechnology, a recent and exciting field of science, allows for advanced research in a variety of fields, including biotechnology, agriculture, and the treatment of a variety of infectious microbial diseases. (Wang et al., 2017; Zulfiqar et al., 2019). We synthesized ZnO-NPs from eucalyptus leaves by using ZnO salt (Ahmad et al., 2020). The environmentally friendly green synthesis of ZnO-NPs with eucalyptus is a safe, non-toxic, low-cost process. The results of Elumalai et al. are refuted by our findings [15], Salgado et al., 2019, Ahmad et al., 2020 who reported that biological synthesis of NPs by using the plant is a fast, eco-friendly, low-cost option and is safe for human use.

We indicated a change in color of the salt solution with plant extract during nanoparticle synthesis. These findings are consistent with Ahmad et al., 2020, who stated that the shift in colour of the solution from colourless to pale yellow was caused by the phenomenon of resonance and absorption transitions processes, which is thought to be the primary indicator of ZnO-NPs synthesis. (Ahmad et al., 2020). FT-IR, XRD, and UV–vis analysis demonstrated that the UV absorption peak observed at 421 nm clearly shows the synthesis of ZnO-NPs (Kumar et al., 2013). FT-IR studies confirmed the fabrication of ZnO-NPs by the action of different phytochemicals with functional groups present in the plant extract (Shaheen et al., 2020). The XRD patterns have shown the purity, composition usually phase, and nature of the ZnO-NPs and the average particle size was found to be 36 mm which also followed the reported result published by (Fakhari et al., 2019).

From this study, it is obvious that ZnO-NPs exhibited strong antimicrobial activity against pathogenic strains of *E. coli*. Our results are in line with the findings of (Jin and Jin, 2021) Elumalai et al. [15], Singh et al. [16], Ahmad et al. [33], who also reported
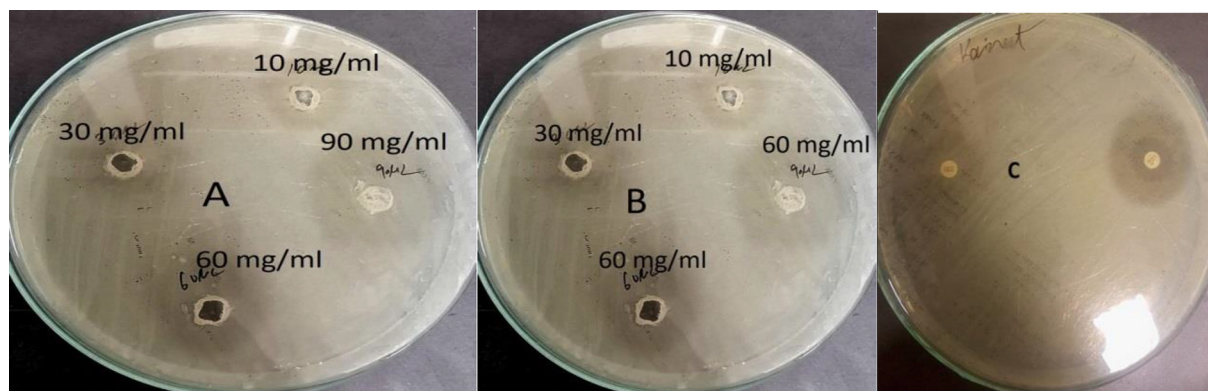
Fig. 7. Antibacterial activities of different concentration of ZnO-NP (10 mg/ml, 30 mg/ml, 60 mg/ml, 90 mg/ml) at A) 12 h. B = 24 h and C = 36 h against pathogenic strain of *E. coli* causing colibacillosis disease of poultry.

Table 6
Parameters used in vina search space for docking.

Center (Å)	Dimensions (Å)
X: −27.5501	X: 65.5753
Y: −0.2162	Y: 62.4444
Z: 50.3675	Z: 57.9704
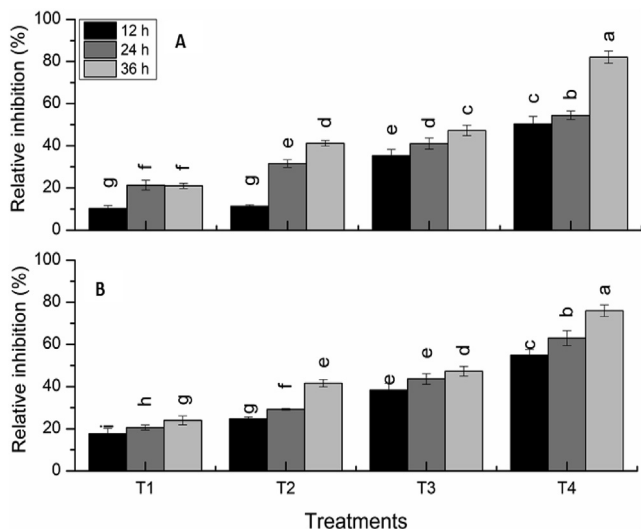
Fig. 8. Relative percentage inhibition of different concentrations of ZnO-NPs against bacterial pathogens strain of *E. coli* of colibacillosis disease. Whereas T1 = 10 mg/ml concentration of aqueous nanoparticles suspension T2 = 30 mg/ml, T3 = 60 mg/ml and T4 = 90 mg/ml concentration. Different letters signify significant variations at LSD (P = 0.05), n = 3 and ± indicates standard error between three replicates.
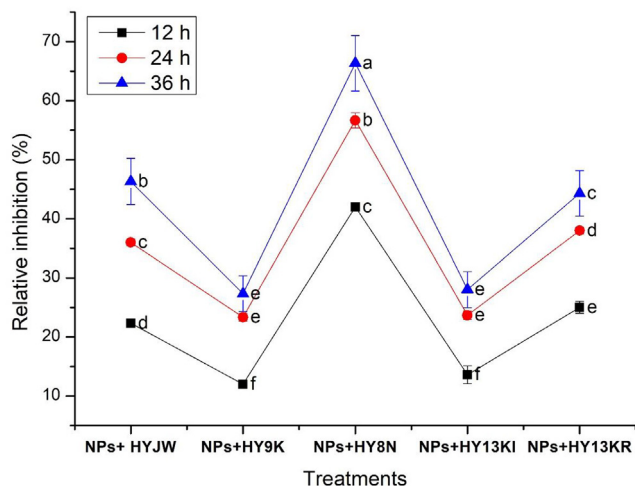
Fig. 9. Relative percentage inhibition of different concentrations of ZnO-NPs (90 mg/ml) in combination with PGPR strains against bacterial pathogens strain of *E. coli* of colibacillosis disease. Details of strains are the same as given in Fig. 4. Different letters signify significant variations at LSD (P = 0.05), n = 3 and ± indicates standard error between three replicates.

that ZnO-NPs show great antimicrobial activity against pathogenic bacteria of animals and plants i.e. *Acinetobacter baumannii,* Campylobacter, E.coli, and some species of Bacillus. Our results demonstrated that the effectiveness of ZnO-NPs depends on its higher concentration and higher incubation time. When maximum concentration (90 mg/ml) of ZnO-NPs was used, greater antibacterial

Table 7
Blind docking of Zinc Oxide nanoparticle with Penicillin-binding protein 6 (PBP6).

Conformation	Binding Residues	Binding Trend	Binding Energy
Frame 1	**Thr210, Gly211, Thr212,** *Arg244,* <u>Ser40, Lys43,</u> Ser82,	**Catalytic Triad,** *Active site,* <u>Catalytic diad,</u> Active site loop 1	−4.3
Frame 2	**Thr210, Gly211,** *Ser106, Asn108,* <u>Ser40, Lys43</u>	**Catalytic Triad,** *(Ser-X-Asn) Motif,* <u>Catalytic Diad</u>	−3.9
Frame 3	**Thr210, Gly211, Thr212,** *Arg244, Phe245,* <u>Ser40, Lys43,</u> Ser82,	**Catalytic Triad,** *Active site,* <u>Catalytic diad,</u> Active site loop 1	−3.9
Frame 4	**Thr210, Gly211, Thr212,** *Arg244, Phe245,* <u>Ser40, Lys43,</u> Ser82, Ser83	**Catalytic Triad,** *Active site,* <u>Catalytic diad,</u> Active site loop 1	−3.8
Frame 5	**Thr210, Gly211, Thr212,** *Arg244,* <u>Ser40, Lys43,</u>	**Catalytic Triad,** *Active site,* <u>Catalytic diad</u>	−3.8
Frame 6	*Ser106, Asn108,* <u>Ser40, Lys43</u>	*(Ser-X-Asn) Motif,* <u>Catalytic Diad</u>	−3.8
Frame 7	*Ser106, Asn108,* <u>Ser40, Lys43,</u> Ser82	*(Ser-X-Asn) Motif,* <u>Catalytic Diad,</u> Active site loop 1	−3.5
Frame 8	**Thr210, Gly211,** *Arg244, Phe245,* <u>Ser40, Lys43</u>	**Catalytic Triad,** *Active site,* <u>Catalytic diad</u>	−3.4
Frame 9	**Thr210, Gly211,** *Arg244,* <u>Ser40, Lys43</u>	**Catalytic Triad,** *Active site,* <u>Catalytic diad,</u>	−3.4

activity of ZnO-NPs (9 mm inhibitory zone) against *E. coli* after 36 h was observedThese findings are consistent with Elumalai et al. (Elumalai et al., 2015) who investigate concentration and incubation time effects on NPs efficiency against pathogenic microorganisms.

Besides the vital role of ZnO-NPs, PGPR also played a role in the growth inhibition of microbes through antagonism. From the results, it is obvious that PGPR had strong antagonism against *E. coli.* The PGPR strains used in present study i.e. *Pseudomonas* sp. (HY8N), *Bacillus pumilus* (HYJW), *Bacillus cereus* (HY9K), *Pseudomonas* sp. (HY13KI), and *Pseudomonas* sp. (HY13KR) showed an increase in growth promotion and drought tolerance in maize (Yasmin et al., 2017a). However, information was lacking about the antimicrobial role of these PGPR strains against animal pathogens. Here for the first time, we observed that *Pseudomonas* sp. (HY8N) showed 67% antagonism against *E. coli* causing colibacillosis disease. The role of PGPR as a biocontrol agent against phytopathogens is well established (Oleńska et al., 2020; Sabaté et al., 2017). They produce hydrolytic enzymes like pectinase, amylase and glucanase, antibiotics, hydrogen cyanide, and other secondary metabolites that inhibit the growth of bacterial and fungal pathogens (Yasmin et al., 2020).

Information was also lacking about the antimicrobial role of these PGPRs strains along with ZnO-NPs against animal pathogens. Here for the first time, we observed that *Pseudomonas* sp. (HY8N) showed 69% antagonism along with ZnO-NPs against *E. coli* causing colibacillosis disease. The significant finding of current study was the synergistic effect of ZnO-NPs to enhance the potential of antagonistic potential of PGPRs. All five PGPR strains when applied with ZnO-NPs (90 mg/ml) exhibited higher growth inhibition of *E. coli* of as compared to its alone application.

In this research, we used *in silico* analysis to better understand the mechanisms that cause antagonism in ligand-receptor interactions. The nanoparticle (ligands) attached to tested *E. coli* strain (receptor PBP 6) with different binding energies. For the *in-silico* analysis of ZnO components with receptor PBP 6, molecular docking was done. For molecular docking, we used 1 ligand and docked with receptor protein penciling binding protein to check the

Fig. 10. ZnO-NPs interaction with PBP6 in 9 frames. Red residues indicate hydrophobic interactions, atomic residues indicate hydrogen bond interactions.

binding of this ligand with penciling binding protein. For doing this we used kcal/mol different software (Allen et al., 2017).

In this research, by using PyRx Autodock vina molecular docking was done for PBP6 receptor and ZnO-NPs. Molecular docking studies provided the best understanding of interactions between ligand and receptor PBP 6. Fig. 9 shows how ZnO-NPs bind to the same binding pockets as previously mentioned in the literature. (Chen et al., 2009). It can be observed that the binding interactions of ZnO-NPs are like the binding trend of PBP6 with other substrates. Also, the β-Lactam compounds present interactions with (Ser-X-Asn) Motif residues Ser106, Asn108, and catalytic triad residues. Therefore, it can be postulated that catalytic triad, catalytic dyad, active site loop1, loop2, (Ser-X-Asn) Motifs can be very useful in the design process. binding of different substrates with PBP 6 (Chen et al., 2009). So, according to the interactions it can be concluded that ZnO-NPs forms the same interaction pattern with respect to other reported ligands, hence it can play an important role in the inhibition of PBP 6.

5. Conclusion

In conclusion, ZnO-NPs showed strong antimicrobial activity at 90 mg/ml concentration against *E. coli* of Colibacillosis disease. Moreover, PGPR strain *Pseudomonas* sp. (HY8N) exhibited successful antagonism against the pathogenic strain of colibacillosis disease. *In silico* studies showed that the mechanism of action for the antagonism is through ligand-receptor binding. However, their antagonistic activity is something that needs to be looked at further for a complete understanding of underlying mechanisms.

Therefore, green synthesized ZnO-NPs and *Pseudomonas* sp. (HY8N) can be significantly used as an alternate poultry medicine and needs to be tested on poultry to observe their efficacy.

Declaration of Competing Interest

The authors declare that they have no known competing financial interests or personal relationships that could have appeared to influence the work reported in this paper.

Acknowledgments

Reference

Zakeri, Afshin, 2012. Antimicrobial susceptibilities of avian Escherichia coli isolates in Tabriz, Iran. AFRICAN J. Biotechnol. https://doi.org/10.5897/ajb11.3168.
Ahmad, H., Venugopal, K., Rajagopal, K., De Britto, S., Nandini, B., Pushpalatha, H.G., Konappa, N., Udayashankar, A.C., Geetha, N., Jogaiah, S., 2020. Green synthesis and characterization of zinc oxide nanoparticles using eucalyptus globules and their fungicidal ability against pathogenic fungi of apple orchards. Biomolecules. https://doi.org/10.3390/biom10030425.
Allen, T.W., Bradley, C.A., Sisson, A.J., Byamukama, E., Chilvers, M.I., Coker, C.M., Collins, A.A., Damicone, J.P., Dorrance, A.E., Dufault, N.S., Esker, P.D., Faske, T.R., Giesler, L.J., Grybauskas, A.P., Hershman, D.E., Hollier, C.A., Isakeit, T., Jardine, D. J., Kelly, H.M., Kemerait, R.C., Kleczewski, N.M., Koenning, S.R., Kurle, J.E., Malvick, D.K., Markell, S.G., Mehl, H.L., Mueller, D.S., Mueller, J.D., Mulrooney, R.

P., Nelson, B.D., Newman, M.A., Osborne, L., Overstreet, C., Padgett, G.B., Phipps, P.M., Price, P.P., Sikora, E.J., Smith, D.L., Spurlock, T.N., Tande, C.A., Tenuta, A.U., Wise, K.A., Wrather, J.A., 2019. Soybean Yield Loss Estimates Due to Diseases in the United States and Ontario, Canada, from 2010 to 2014. Plant Heal. Prog. 18, 19–27. https://doi.org/10.1094/PHP-RS-16-0066.

Beneduzi, A., Ambrosini, A., Passaglia, L.M.P., 2012. Plant growth-promoting rhizobacteria (PGPR): Their potential as antagonists and biocontrol agents. Genet. Mol. Biol. 35, 1044–1051.

Berman, H.M., Bhat, T.N., Bourne, P.E., Feng, Z., Gilliland, G., Weissig, H., Westbrook, J., 2000. The Protein Data Bank and the challenge of structural genomics. Nat. Struct. Biol. https://doi.org/10.1038/80734.

Chen, Y., Zhang, W., Shi, Q., Hesek, D., Lee, M., Mobashery, S., Shoichet, B.K., 2009. Crystal structures of penicillin-binding protein 6 from Escherichia coli. J. Am. Chem. Soc. https://doi.org/10.1021/ja903773f.

Chouhan, S., Sharma, K., Guleria, S., 2017. Antimicrobial Activity of Some Essential Oils-Present Status and Future Perspectives. Med. (Basel, Switzerland) 4, 58. https://doi.org/10.3390/medicines4030058

Coura, F.M., Diniz, S.A., Silva, M.X., Arcebismo, T.L.M., Minharro, S., Feitosa, A.C.F., Lage, A.P., Knöbl, T., Mussi, J.M.S., Heinemann, M.B., 2017. Phylogenetic Group of Escherichia coli Isolates from Broilers in Brazilian Poultry Slaughterhouse. World J. Sci. https://doi.org/10.1155/2017/5898701.

Dadi, R., Azouani, R., Traore, M., Mielcarek, C., Kanaev, A., 2019. Antibacterial activity of ZnO and CuO nanoparticles against gram positive and gram negative strains. Sci. Eng. C Mater. https://doi.org/10.1016/j.msec.2019.109968.

Dellacassa, E., Menéndez, P., Moyna, P., Soler, E., 1990. Chemical composition of Eucalyptus essential oils grown in Uruguay. Flavour Fragr. J. https://doi.org/10.1002/ffj.2730050207.

Elumalai, K., Velmurugan, S., Ravi, S., Kathiravan, V., Ashokkumar, S., 2015. Green synthesis of zinc oxide nanoparticles using Moringa oleifera leaf extract and evaluation of its antimicrobial activity. Acta - Part A Mol. Biomol. Spectrosc. Spectrochim. https://doi.org/10.1016/j.saa.2015.02.011.

Fakhari, S., Jamzad, M., Kabiri Fard, H., 2019. Green synthesis of zinc oxide nanoparticles: a comparison. Green Chem. Lett. Rev. https://doi.org/10.1080/17518253.2018.1547925

Farhangi-Abriz, S., Torabian, S., 2018. Nano-silicon alters antioxidant activities of soybean seedlings under salt toxicity. Protoplasma. https://doi.org/10.1007/s00709-017-1202-0

Furqan, T., Batool, Sidra, Habib, R., Shah, M., Kalasz, H., Darvas, F., Kuca, K., Nepovimova, E., Batool, S., Nurulain, S.M., 2020. Cannabis constituents and acetylcholinesterase interaction: Molecular docking, in vitro studies and association with CNR1 RS806368 and ACHE RS17228602. Biomolecules. https://doi.org/10.3390/biom10050758.

Ghosh, A., Chowdhury, C., Nelson, D., 2008. Physiological functions of D-alanine carboxypeptidases in Escherichia coli. Trends Microbiol. 16, 309–317. https://doi.org/10.1016/j.tim.2008.04.006.

Habibi, H., Ghahtan, N., Morammazi, S., 2018. The effects of some herbal essential oils against Salmonella and Escherichia coli isolated from infected broiler flocks. J. World's Poult. Res.

Heredia, N., García, S., 2018. Animals as sources of food-borne pathogens: A review. Nutr. Anim. https://doi.org/10.1016/j.aninu.2018.04.006.

Ibrahim, R.A., Cryer, T.L., Lafi, S.Q., Basha, E.A., Good, L., Tarazi, Y.H., 2019. Identification of Escherichia coli from broiler chickens in Jordan, their antimicrobial resistance, gene characterization and the associated risk factors. BMC Vet. Res. https://doi.org/10.1186/s12917-019-1901-1.

Jamil, B., Abbasi, R., Abbasi, S., Imran, M., Khan, S.U., Ihsan, A., Javed, S., Bokhari, H., 2016. Encapsulation of cardamom essential oil in chitosan nano-composites: In-vitro efficacy on antibiotic-resistant bacterial pathogens and cytotoxicity studies. Front. Microbiol. https://doi.org/10.3389/fmicb.2016.01580.

Jin, S.-E., Jin, H.-E., 2021. Antimicrobial Activity of Zinc Oxide Nano/Microparticles and Their Combinations against Pathogenic Microorganisms for Biomedical Applications: From Physicochemical Characteristics to Pharmacological Aspects. Nanomater. https://doi.org/10.3390/nano11020263.

Kim, H.M., Park, J.H., Lee, S.K., 2019. Fiber optic sensor based on ZnO nanowires decorated by Au nanoparticles for improved plasmonic biosensor. Sci. Rep. https://doi.org/10.1038/s41598-019-52056-1.

Kumar, S.S., Venkateswarlu, P., Rao, V.R., Rao, G.N., 2013. Synthesis, characterization and optical properties of zinc oxide nanoparticles. Int. Nano Lett. https://doi.org/10.1186/2228-5326-3-30.

Macheboeuf, P., Contreras-Martel, C., Job, V., Dideberg, O., Dessen, A., 2006. Penicillin Binding Proteins: key players in bacterial cell cycle and drug

resistance processes. FEMS Microbiol. Rev. 30, 673–691. https://doi.org/10.1111/j.1574-6976.2006.00024.x.

Millezi, A.F., Costa, K.A.D., Oliveira, J.M., Lopes, S.P., Pereira, M.O., Piccoli, R.H., 2019. Antibacterial and anti-biofilm activity of cinnamon essential oil and eugenol. Cienc. Rural. https://doi.org/10.1590/0103-8478CR20180314.

Nukaga, M., Bethel, C.R., Thomson, J.M., Hujer, A.M., Distler, A., Anderson, V.E., Knox, J.R., Bonomo, R.A., 2008. Inhibition of class a β-lactamases by carbapenems: Crystallographic observation of two conformations of meropenem in SHV-1. J. Am. Chem. Soc. https://doi.org/10.1021/ja7111146.

Oleńska, E., Małek, W., Wójcik, M., Swiecicka, I., Thijs, S., Vangronsveld, J., 2020. Beneficial features of plant growth-promoting rhizobacteria for improving plant growth and health in challenging conditions: A methodical review. Sci. Total Environ. https://doi.org/10.1016/j.scitotenv.2020.140682.

Sabaté, D.C., Pérez Brandan, C., Petroselli, G., Erra-Balsells, R., Audisio, M.C., 2017. Decrease in the incidence of charcoal root rot in common bean (Phaseolus vulgaris L.) by Bacillus amyloliquefaciens B14, a strain with PGPR properties. Biol. Control 113, 1–8. https://doi.org/10.1016/j.biocontrol.2017.06.008.

Salgado, P., Mártire, D.O., Vidal, G., 2019. Eucalyptus extracts-mediated synthesis of metallic and metal oxide nanoparticles: Current status and perspectives. Mater. Res. Exp. https://doi.org/10.1088/2053-1591/ab254c.

Sánchez-López, E., Gomes, D., Esteruelas, G., Bonilla, L., Lopez-Machado, A.L., Galindo, R., Cano, A., Espina, M., Ettcheto, M., Camins, A., Silva, A.M., Durazzo, A., Santini, A., Garcia, M.L., Souto, E.B., 2020. Metal-based nanoparticles as antimicrobial agents: An overview. Nanomaterials. https://doi.org/10.3390/nano10020292.

Sauvage, E., Kerff, F., Terrak, M., Ayala, J.A., Charlier, P., 2008. The penicillin-binding proteins: structure and role in peptidoglycan biosynthesis. FEMS Microbiol. Rev. 32, 234–258. https://doi.org/10.1111/j.1574-6976.2008.00105.x.

Shaheen, I., Ahmad, K.S., Jaffri, S.B., Ali, D., 2020. Biomimetic [MoO3@ZnO] semiconducting nanocomposites: Chemo-proportional fabrication, characterization and energy storage potential exploration. Renew. Energy. https://doi.org/https://doi.org/10.1016/j.renene.2020.11.115

Singh, A., Singh, N.B., Afzal, S., Singh, T., Hussain, I., 2018. Zinc oxide nanoparticles: a review of their biological synthesis, antimicrobial activity, uptake, translocation and biotransformation in plants. J. Mater. Sci. https://doi.org/10.1007/s10853-017-1544-1.

Spratt, B.G., Strominger, J.L., 1976. Identification of the major penicillin binding proteins of Escherichia coli as D alanine carboxypeptidase IA. J. Bacteriol. https://doi.org/10.1128/jb.127.1.660-663.1976.

Tamura, T., Imae, Y., Strominger, J.L., 1976. Purification to homogeneity and properties of two D alanine carboxypeptidases I from Escherichia coli. J. Biol. Chem. https://doi.org/10.1016/S0021-9258(17)33895-4.

Vecchio, M.G., Loganes, C., Minto, C., 2016. Beneficial and Healthy Properties of Eucalyptus Plants: A Great Potential Use. Open. Agric. J. https://doi.org/10.2174/1874331501610010052.

Wang, L., Hu, C., Shao, L., 2017. The antimicrobial activity of nanoparticles: Present situation and prospects for the future. Int. J. Nanomed. https://doi.org/10.2147/IJN.S121956.

Xing, Z., Li, H., Li, M., Gao, R., Guo, C., Mi, S., 2020. Disequilibrium in chicken gut microflora with avian colibacillosis is related to microenvironment damaged by antibiotics. Sci. Total Environ. https://doi.org/10.1016/j.scitotenv.2020.143058.

Yang, H., Zou, H., Chen, M., Li, S., Jin, J., Ma, J., 2017. The green synthesis of ultrafine palladium–phosphorus alloyed nanoparticles anchored on polydopamine functionalized graphene used as an excellent electrocatalyst for ethanol oxidation. Inorg. Chem. Front.. https://doi.org/10.1039/c7qi00394c.

Yasmin, H., Naz, R., Nosheen, A., Hassan, M.N., Ilyas, N., Sajjad, M., Anjum, S., Gao, X., Geng, Z., 2020. Identification of New Biocontrol Agent against Charcoal Rot Disease Caused by Macrophomina phaseolina in Soybean (Glycine max L.). Sustainability 12, 6856.

Yasmin, H., Nosheen, A., Naz, R., Bano, A., Keyani, R., 2017a. L-tryptophan-assisted pgpr-mediated induction of drought tolerance in maize (Zea mays L.). J. Plant Interact. 12, 567–578. https://doi.org/10.1080/17429145.2017.1402212.

Yasmin, H., Nosheen, A., Naz, R., Bano, A., Keyani, R., Zea, L., 2017b. l-tryptophan-assisted PGPR-mediated induction of drought tolerance in maize (Zea mays L.) PGPR-mediated induction of drought tolerance in maize 9145. https://doi.org/10.1080/17429145.2017.1402212.

Zulfiqar, F., Navarro, M., Ashraf, M., Akram, N.A., Munné-Bosch, S., 2019. Nanofertilizer use for sustainable agriculture: Advantages and limitations. Plant Sci. https://doi.org/10.1016/j.plantsci.2019.110270.